Supporting Information

Mn-doping method boosts Se doping concentration in Cu_2S towards high thermoelectric performance

*Chen Gong, Zhiwei Zeng, Xiaoling Sun, Chengran Luo, Hongyi Chen**

C Gong, Z Zeng, X Sun, C Luo, H Chen*

Central South University

College of Chemistry and Chemical Engineering

Central South University

Changsha 410083, China

E- mail: hongyichen@csu.edu.cn

Supplementary Index

Supplementary Text

S1. Single parabolic band (SPB) model.

$$L = (\frac{k_B}{e})^2 \times \left\{ \frac{(3+\lambda_\tau)F_{2+\lambda_\tau}(\eta)}{(1+\lambda_\tau)F_{\lambda_\tau}(\eta)} - \left[\frac{(2+\lambda_\tau)F_{1+\lambda_\tau}(\eta)}{(1+\lambda_\tau)F_{\lambda_\tau}(\eta)} \right]^2 \right\} \quad (1)$$

$$\alpha = \frac{k_B}{e}\left[\frac{\left((2+\lambda_\tau)F_{1+\lambda_\tau}(\eta)\right)}{(1+\lambda_\tau)F_{\lambda_\tau}(\eta)} - \eta \right] \quad (2)$$

$$n = \frac{4\pi\left(2m^* k_B T\right)^{3/2}}{h^2} F_{1/2}(\eta) \quad (3)$$

$$F_i(\eta) = \int_0^\infty \frac{\xi}{1+exp(\xi-\eta)} d\xi \quad (4)$$

In the above equations, (4) is the Fermi integral, $\eta = E_F/K_BT$ is the reduction Fermi energy, ξ is the reduction carrier energy, K_b is Boltzmann's constant, e is the electron charge, h is Planck's constant, m^* is the effective mass, λ_τ is the scattering factor and its value is 0. *L* is the Lorentz constant.

S2. Calculation of estimated optical band gap

$$(\varepsilon h\nu)^{1/m} = B(h\nu - E_g) \quad (5)$$

where ε is the absorption coefficient, h is Planck constant, ν is the incident photon frequency, B is the proportionality constant, and E_g is the band gap. *m* is related to the properties of semiconductor materials, *m*=2 was used for Tauc plot analysis. Based on Lambert-Beer's law:

$A = K\varepsilon$ (6)

where *A* is the absorbance of the sample and K is a proportionality constant independent of absorbance. Putting the Lambert-Beer formula into equation (5), we can get formula :

$$(A h\nu)^{1/m} = BK^{1/m}(h\nu - E_g) \quad (7)$$

Let $BK^{1/m}$ be a constant C, A be a *F(R)*, which is:

$$(F(R) h\nu)^{1/m} = C(h\nu - E_g) \quad (8)$$

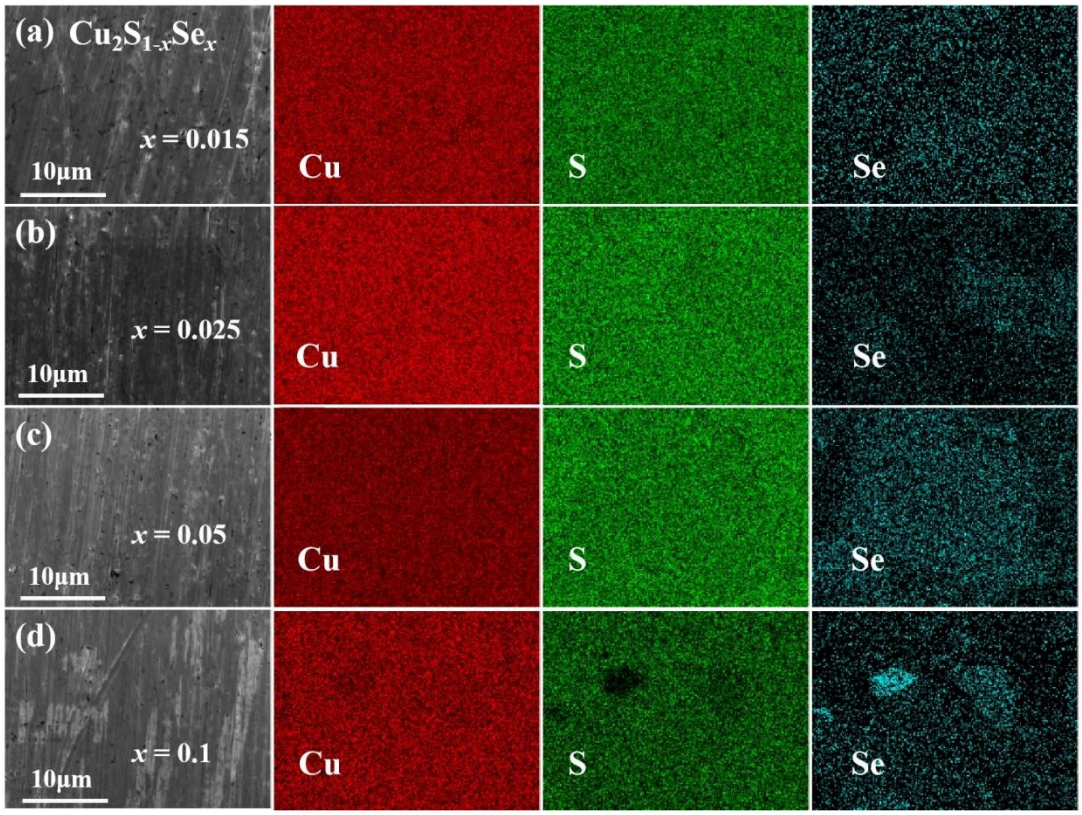

Fig. S1. SEM images and the EDS mapping for Cu, S, Mn and Se for $Cu_2S_{1-x}Se_x$ (a) x = 0.015, (b) x = 0.025, (c) x =0 .05, (d) x = 0.1.

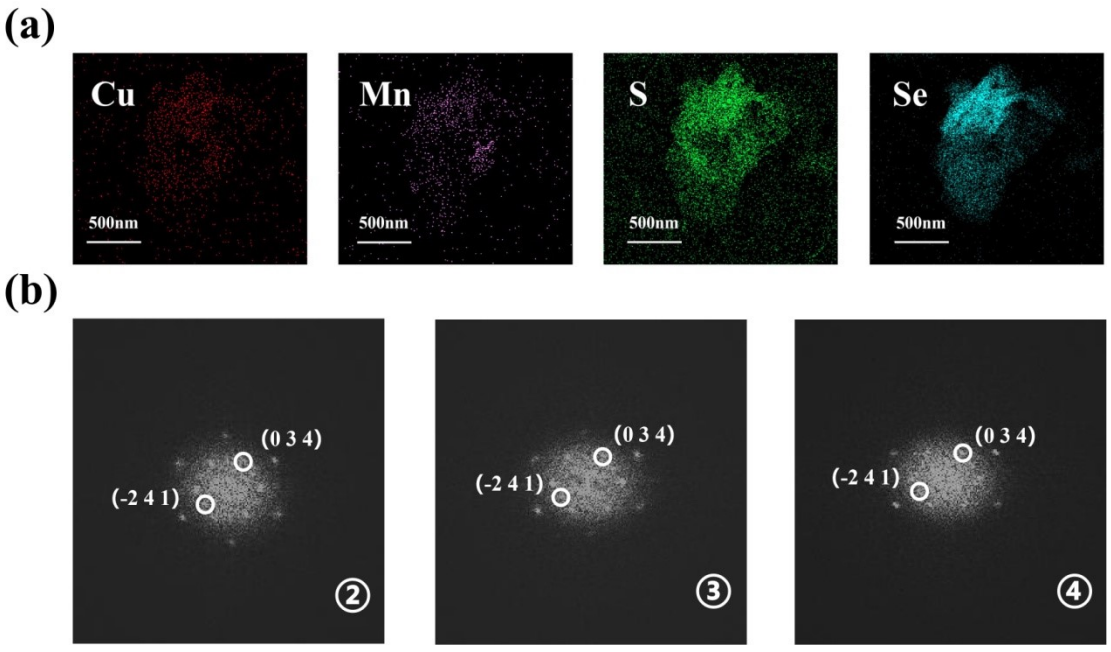

Fig. S2. Microstructure for $Cu_{1.96}Mn_{0.02}S_{0.975}Se_{0.025}$.(a) The elemental EDS mapping of $Cu_{1.96}Mn_{0.02}S_{0.975}Se_{0.025}$. (b) The fast Fourier transform (FFT) patterns for 2, 3, 4 regions in high-magnification TEM image of$Cu_{1.96}Mn_{0.02}S_{0.975}Se_{0.025}$.

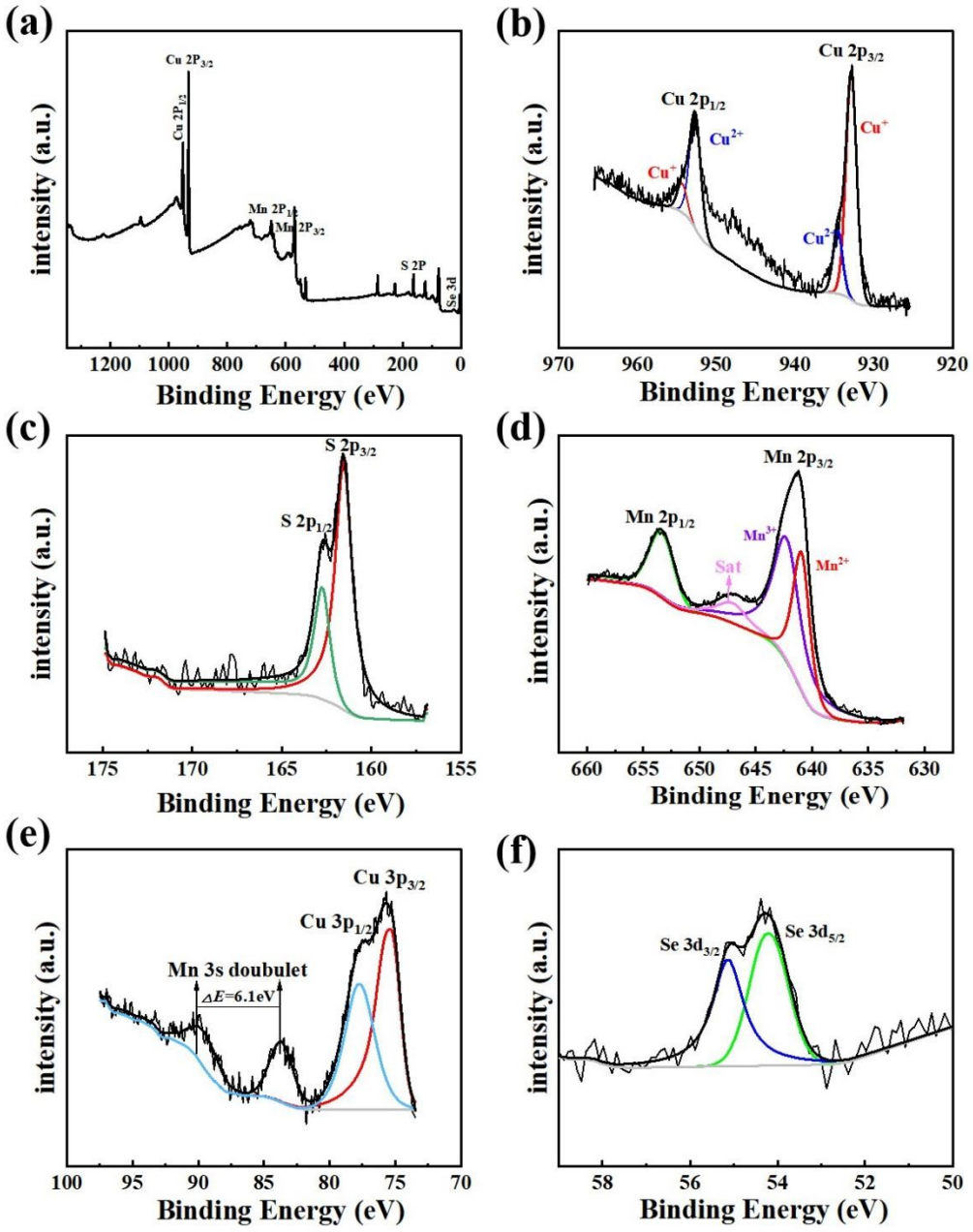

Fig. S3. The X-ray photoelectron spectroscopy (XPS) for $Cu_{1.96}Mn_{0.02}S_{0.975}Se_{0.025}$. (a) Comprehensive XPS scanning of $Cu_{1.96}Mn_{0.02}S_{0.975}Se_{0.025}$ sample. (b) The core states of Cu $2p_{1/2}$ and $2p_{3/2}$.(c) S $2p_{1/2}$ and S $2p_{3/2}$ cores. (d) The core states of Mn $2p_{1/2}$ and $2p_{3/2}$.(e) The core states of Mn 3s.The energy value of the 3s splitting peak of $Mn^{2+}$is 6eV. (f) $Se3d_{3/2}$ and $Se3d_{5/2}$ cores.

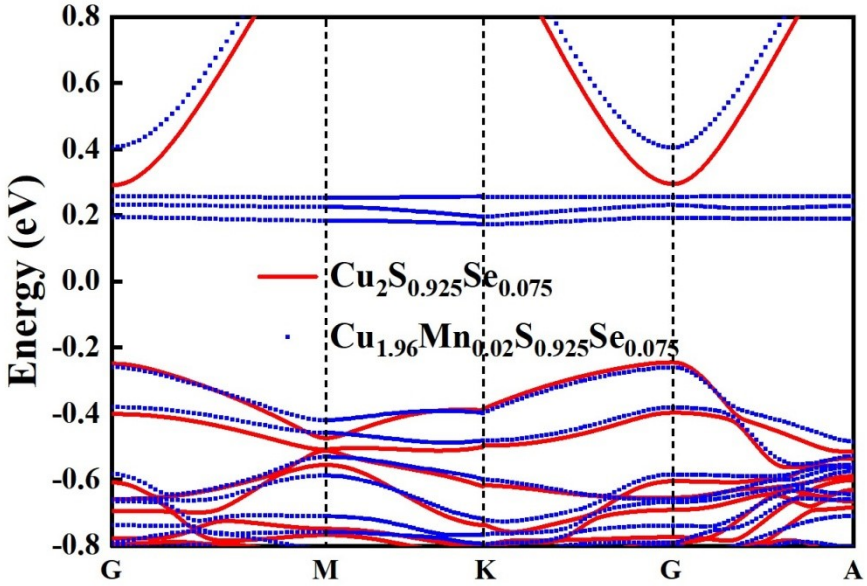

Fig. S4. The calculated electronic band structures for the $Cu_2S_{0.925}Se_{0.075}$ and $Cu_{1.96}Mn_{0.02}S_{0.925}Se_{0.075}$.

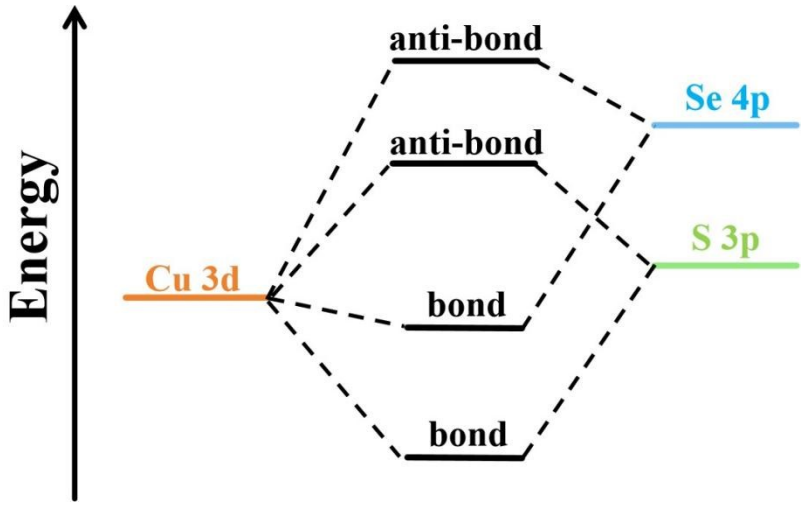

Fig. S5. Schematic atomic orbital hybridization diagram of Se doping in Cu_2S.

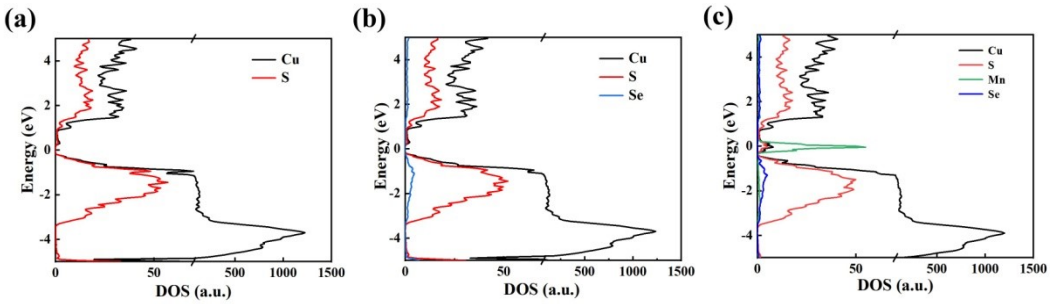

Fig. S6. The pDOS of (a) Cu_2S. (b) $Cu_2S_{0.925}Se_{0.075}$. (c) $Cu_{1.96}Mn_{0.02}S_{0.925}Se_{0.075}$.

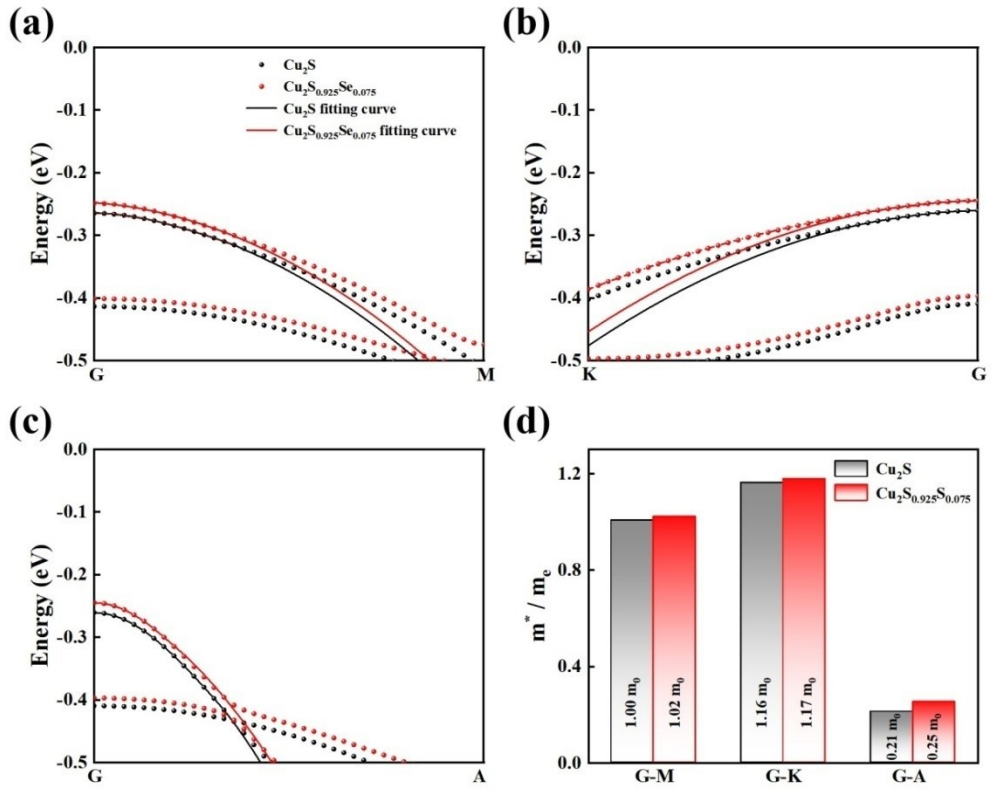

Fig. S7. The curvature of the fitting the electronic band structures for the Cu_2S and $Cu_2S_{0.925}Se_{0.075}$ in (a) G - M(1 0 0), (b) G - K(1 1 0) and (c) G - A(0 0 1). Effective mass for the Cu_2S and $Cu_2S_{0.925}Se_{0.075}$ in G - M(1 0 0), G - K(1 1 0), G - A(0 0 1).

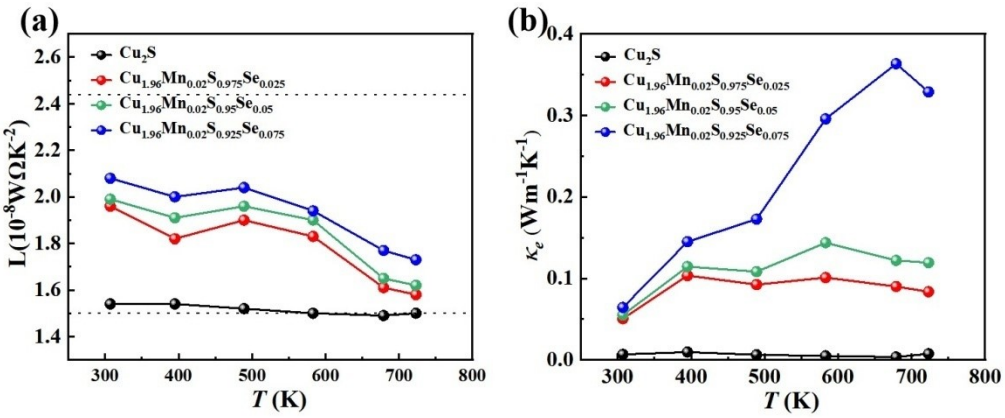

Fig. S8. Temperature dependence of (a) Lorentz constant, and(b) Electronic thermal conductivity (κ_e).

The Vickers hardness and compressive stress of the $Cu_{1.96}Mn_{0.02}S_{0.95}Se_{0.05}$ were tested as shown in Fig. S8. The Vickers hardness of our material is 59.3 *H*v, which is at a medium level compared to other thermoelectric materials. When the compressive stress reaches about 96 Mpa, the compression limit of the sample is 35%, and more pressure is applied, the sample is completely shattered. The Vickers hardness test and compressive stress test showed good mechanical properties of the sample.

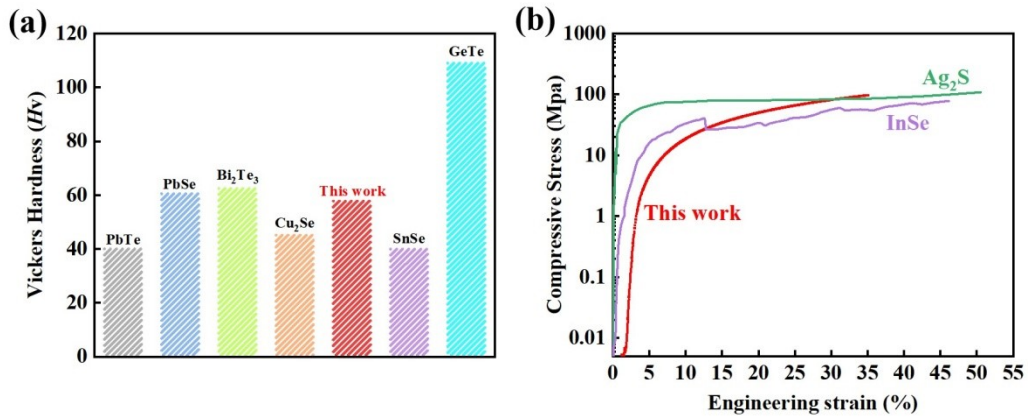

Fig. S9. (a) The Vickers hardness comparison of popular thermoelectric materials. (b) The compression stress curve of $Cu_{1.96}Mn_{0.02}S_{0.95}Se_{0.05}$ and other typical TE materials.

The cyclic test on the best performance sample $Cu_{1.96}Mn_{0.02}S_{0.95}Se_{0.05}$ are carried out. Based on the results of the tests, our materials have good heating and cooling cycle performance.

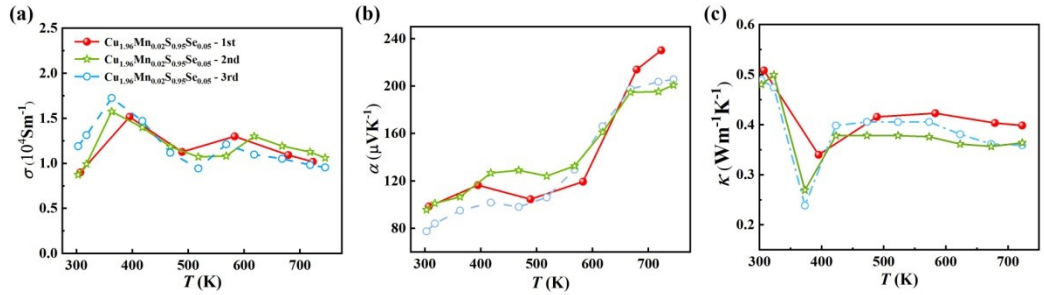

Fig. S10. Heating and cooling cycle test of $Cu_{1.96}Mn_{0.02}S_{0.95}Se_{0.05}$. (a) Electrical conductivity σ. (b) Seebeck coefficient α. (c) thermal conductivity κ.

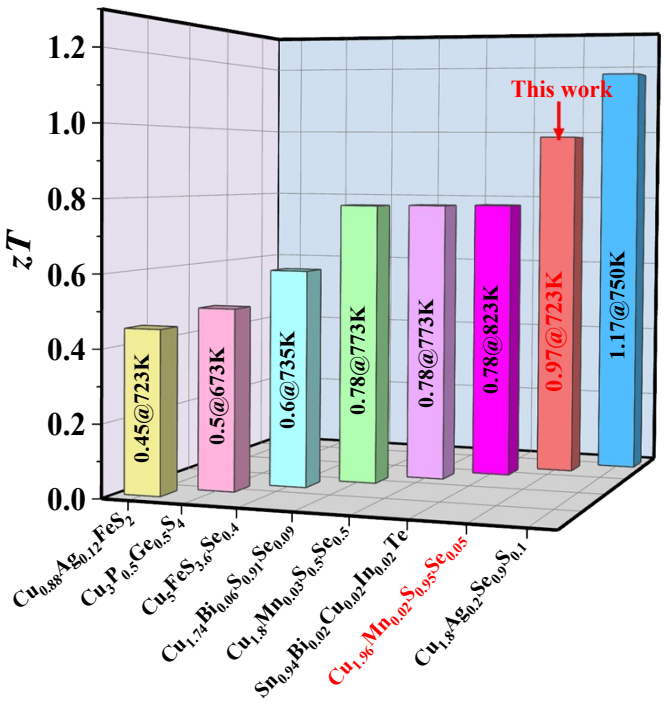

Fig. S11. Comparison of *zT* for $Cu_{1.96}Mn_{0.02}S_{0.95}Se_{0.05}$ with other class of high performing typical copper based TE materials containing multiple dopants.